Impact of Al2O3, TiO2 and ZnO addition on the crystallization of Yb3+ doped phosphate glass-ceramic

Mikko Hongisto, Otto Linros, Sylvain Danto, Veronique Jubera, Laeticia Petit

HAL Id: hal-03778423

https://hal.science/hal-03778423

Submitted on 15 Sep 2022

Research Papers

Impact of Al$_2$O$_3$, TiO$_2$ and ZnO addition on the crystallization of Yb^{3+} doped phosphate glass-ceramic

Mikko Hongisto [a,b,*], Otto Linros [a], Sylvain Danto [b], Veronique Jubera [b], Laeticia Petit [a]

[a] Photonics Laboratory, Tampere University, Korkeakoulunkatu 3, 33720, Tampere, Finland
[b] Univ. Bordeaux, CNRS, Bordeaux INP, ICMCB, UMR 5026, F-33600 Pessac, France

ABSTRACT

New Yb^{3+}-doped phosphate glasses with a composition of (98.75-x) (90 NaPO$_3$ – 10 Na$_2$O) – x (Al$_2$O$_3$, TiO$_2$, or ZnO) – 1.25 Yb$_2$O$_3$ (in mol-%), with x from 0 to 3, were prepared via conventional melting and quenching process. The thermal and physical properties were studied by differential thermal analysis (DTA) and density measurement, respectively. The glass structure was investigated using visible/infrared spectroscopy and the crystallization properties of the glasses using XRD. Changes in the glass composition were found to have an impact on the glass structure and more importantly on the crystallization process; the addition of Al$_2$O$_3$, TiO$_2$ and ZnO promotes the precipitation of the Na$_5$P$_3$O$_{10}$ crystalline phase at the expense of NaYb(P$_2$O$_7$) and NaPO$_3$ phases and more importantly, promotes surface crystallization at the expense of bulk crystallization.

1. Introduction

Yb^{3+} ion is a rare-earth (RE) ion of interest since it has a favorable energy level structure for high power laser amplifiers [1–3]. Indeed, it possesses a very low quantum defect in comparison with Nd^{3+} ions and a direct excitation of the ^{2}F$_{5/2}$ level can be efficiently achieved with high power and efficiency InGaAs commercial laser diodes. In addition, its simple energy diagram results in a lack of cross-relaxation mechanisms in Yb^{3+} doped materials, allowing a higher doping **concentration than other RE-doped glasses** and thus **larger** potential effective emission cross-section **before RE concentration quenching begins to affect the emission lifetime and intensities [4, 5]**. Thus, the lack of excited levels at higher energy limits the up-conversion process or absorption into the excited state (ESA phenomenon). However, for high Yb^{3+} content, it is possible, under IR irradiation, to detect a blue luminescence which can be attributed to cooperative luminescence. This process results from simultaneous de-excitation of two neighboring Yb^{3+} ions and a visible emission from a virtual level located at about 20 000 cm^{-1} [6, 7]. When incorporated into glass, the discrimination between the different ^{2}F$_{5/2}$–^{2}F$_{7/2}$ lines is generally not possible because of a global broadening of the emission spectral distribution [2,8].

Majority of the commercial Yb^{3+} doped fiber lasers are made from silica glass which is constructed around a 3D-silicon dioxide network. While this 3D network provides good mechanical and chemical properties, the solubility of Yb^{3+} ions in this glass network is rather low, leading to the formation of Yb-Yb clusters at high Yb$_2$O$_3$ doping levels

[9]. In comparison, phosphate glasses enable high RE-ion solubility, luminescence quenching phenomenon in phosphate glasses occurring at high concentrations of RE [10]. Thus, Yb^{3+}-doped phosphate glasses have become significant alternatives to silica glass in efficient, high-power lasers [11].

It is commonly known that the spectroscopic properties of RE strongly depend on their local crystal field and thus can be enhanced by locating the RE-ions into a nano/microcrystal of specific composition embedded in a glass matrix [12]. Heat-treatment is commonly used to prepare glass-ceramic from glass. The RE containing nano/microcrystals should be distributed homogeneously in the glass volume to insure isotropic and good optical properties, so that the glass-ceramic is considered as a promising material for photonic applications.

Although many studies have been published on Er^{3+} doped transparent glass-ceramics [13–17], fewer studies have been reported on transparent Yb^{3+} doped glass-ceramics, especially on phosphate glass-ceramics [12,17-21]. For example, transparent glass-ceramic was successful prepared from a YbF$_3$ -doped 50 SiO$_2$ – 10 Al$_2$O$_3$ – 20 ZnF$_2$ – 20 SrF$_2$ (mol-%) fluorosilicate glass. After a 2-hour thermal treatment at the first peak crystallization temperature, an increase in the effective Yb^{3+} emission bandwidth and in the upper state Yb^{3+} lifetime was reported due to the glass-to-crystal phase transformation process in due to changes in the crystal-field surrounding Yb^{3+} ions as the Yb^{3+} ions entered in the SrF$_2$ nanocrystals formed during the thermal treatment [17]. Yb^{3+} doped aluminosilicate oxyfluoride glass-ceramics have been investigated for laser cooling applications, for example [19, 20]. Soares

---

* Corresponding author.
  E-mail address: mikko.hongisto@tuni.fi (M. Hongisto).

de Lima Filho *et.al.* in [19] investigated the precipitation of Yb^{3+} doped PbF$_2$ nanocrystals in the glass with the composition 30 SiO$_2$ – 15 Al$_2$O$_3$ – 25 CdF$_2$ – 22 PbF$_2$ – 4 YF$_3$ – 2 YbF$_3$ (mol-%) glass after heat treatment for 30 h at ~10 °C above the peak crystallization temperature. It was found that the quantum efficiency of the Yb^{3+} emission increased up to 10% in the glass-ceramic compared to untreated glass. Similar increase in quantum efficiency was also reported by Meyneng *et.al.* in the 37.6 SiO$_2$ - 22.4 Al$_2$O$_3$ - 19YF$_3$ - 20 LiF - 1 YbF$_3$ (mol-%) glass after heat treatment at 60 °C above the glass transition temperature for 7 h. The increased Yb^{3+} emission quantum efficiency was attributed to precipitation of Yb^{3+} -doped YF$_3$ and/or YLiF$_4$ nanocrystals [20]. Luo *et.al.* successfully prepared Yb^{3+} doped ZnO -containing aluminosilicate glass-ceramic with Yb^{3+} doped ZnO nanocrystals that enabled conversion of UV–Vis to NIR photons [21]. Recently, we reported a study on the crystallization of glasses in the Yb^{3+}-doped NaPO$_3$—Na$_2$O—NaF glass system [18]. It was found that the replacement of Na$_2$O by NaF leads to significant changes in the crystallization process, especially inhibiting the bulk crystallization of NaPO$_3$, Na$_5$P$_3$O$_{10}$ and NaYb(P$_2$O$_7$) crystals occurring during the thermal treatment. A transparent glass-ceramic was successfully prepared from the NaF glass. However, this glass and corresponding glass-ceramic have poor chemical durability and are hygroscopic, drastically limiting their potential use for future applications.

Therefore, the goal of the current study is to tailor the previously researched composition to improve its resistance to water absorption over time and to characterize the effects of composition adjustment on the structural, thermal, and spectroscopic properties together with the glass crystallization behavior. Metal oxides such as Al$_2$O$_3$, TiO$_2$, and ZnO were selected as they are known to increase the durability against water absorption as reported in [22–27]. The impact of adding Al$_2$O$_3$, TiO$_2$, and ZnO in the Yb^{3+}-doped NaPO$_3$–Na$_2$O system is discussed below. **It was found that all additives affect the crystallization and nucleation process with Al$_2$O$_3$ and TiO$_2$ having a noticeable impact on the physical and thermal properties.**

2. Methods

The composition of the investigated glasses is (98.75-x) (90 NaPO$_3$ – 10 Na$_2$O) – x (Al$_2$O$_3$, TiO$_2$, or ZnO) – 1.25 Yb$_2$O$_3$ (in mol-%), with x from 0 to 3. The preparation of the glasses was done using the conventional melting and quenching method. Melting of 6 g batches was performed in platinum crucible between 900 °C and 1100 °C, depending on x. Quenching was performed on a brass plate followed by annealing for 6 h at 40 °C below the respective glass transition temperature of the glasses. Thermal treatment was done after annealing by placing the glass on a Pt plate in a calibrated preheated furnace for a set period of time and temperature.

The raw materials were NaPO$_3$ (Sigma, *tech.*), Na$_2$CO$_3$ (Sigma, ≥99.5%), Al$_2$O$_3$ (Sigma, ≥99%), TiO$_2$ (Sigma, ≥99.8%), ZnO (Sigma, ≥99.99%) and Yb$_2$O$_3$ (Sigma, ≥99.9%).

The glasses' density was assessed by Archimedes' method. Anhydrous ethanol was used for the liquid. Accuracy of measurement is ±0.02 g/cm^3.

Temperatures corresponding to the glass transition temperature (T$_g$), onset of crystallization (T$_x$), and crystallization temperature (T$_p$) were determined with DTA (JUPITER F1, Netzch) using a heating rate of 10 °C/min in N$_2$ atmosphere. The glass transition temperature was obtained as the inflection point of the first endothermic signal and the crystallization temperature at maximum of the exothermic peak. The onset of crystallization was determined as the intersection of the tangent of the exotherm peak with the baseline. A measurement uncertainty of ± 3 °C was determined.

The absorption spectra were obtained with a spectrophotometer (UV-3600 Plus, Shimadzu) from 200 nm to 1100 nm. From the absorption coefficient, the absorption cross-section $\sigma_{abs}(\lambda)$ was computed with Eq. (1).

$$\sigma_{abs}(\lambda) = \frac{\ln 10 \log\left(\frac{I}{I_0}\right)}{NL} \tag{1}$$

where N is the concentration of RE ions per cm^3 based on the measured density and expected composition of the glass, L the thickness of the sample in cm and $\log\left(\frac{I}{I_0}\right)$ the absorbance. Measurement accuracy was ± 10%.

The infrared spectra were obtained with Perkin Elmer Spectrum One FTIR-spectrometer. The absorption spectra were acquired from 3800 cm^{-1} to 2600 cm^{-1} using ~1 mm thick polished glasses. Glasses crushed into powder were used for the IR spectra measured in attenuated total reflectance (ATR) arrangement from 1400 cm^{-1} to 650 cm^{-1}. Data were collected every 4 cm^{-1} and results were accumulated over 8 scans.

The emission spectra were measured with a spectrometer (iHR320, Jobin Yvon), detector (P4631–02, Hamamatsu). A single-mode pigtail diode laser (CM962UF76P-10R, Oclaro) emitting at 965 nm was used for excitation. The samples were crushed into powder for the measurement. The emission cross-section (σ_{emi}) was calculated using equations 2 - 4, adapted from [28,29]:

$$\sigma_{emi} = \frac{\lambda^4 A_R}{8\pi cn^2 \Delta\lambda_{eff}} \tag{2}$$

$$A_R = \frac{8\pi cn^2(2J'+1)}{\lambda_p^4(2J+1)} \int \alpha \, d\lambda \tag{3}$$

$$\Delta\lambda_{eff} = \int \frac{I(\lambda)d\lambda}{I_{max}} \tag{4}$$

where λ is the wavelength, A$_R$ the probability of spontaneous emission, c the speed of light, n the refractive index, here 1.54 [18], $\Delta\lambda_{eff}$ the fluorescence effective linewidth, J' and J correspond to upper and lower level momentums equal to 5/2 and 7/2, respectively, $\int \alpha \, d\lambda$ the integrated absorption cross section, λ_p the wavelength of peak absorption and I(λ) the emission intensity as a function of wavelength. The intensity at the peak wavelength λ is denoted as I$_{max}$.

An X-Ray Diffractometer (EMPYREAN, Panalytical) with cobalt Kα tube (iron filtered, 1.78897 Å) was used to identify the glass-ceramic crystalline phases. Measurements were taken from 15° to 55° at 0.026° intervals.

A scanning electron microscope (SEM) (Leo 1530 Gemini, Zeiss) was used to image the glasses and crystals in the thermally treated glasses.

3. Results and discussion

Glasses with the composition of (98.75-x) (90 NaPO$_3$ – 10 Na$_2$O) – x (Al$_2$O$_3$, TiO$_2$, or ZnO) – 1.25 Yb$_2$O$_3$ (in mol-%), with x from 0 to 3, were prepared in order to investigate the compositional effect on the structural, thermal, and spectroscopic properties of the glass and more importantly of its crystallization process.

The composition and code of the investigated glasses are listed in Table 1, along with their physical and thermal properties.

Within the accuracy of measurement, the compositional changes have no noticeable effect on the density of the glass. While the progressive addition of ZnO does not alter the thermal properties of the glass significantly, the addition of Al$_2$O$_3$ and TiO$_2$ results in an increase in glass transition temperature (T$_g$), crystallization onset temperature (T$_x$), first crystallization peak temperature (T$_p$). The T$_g$ was determined as the inflection point of the endotherm obtained by taking the first derivative of the DTA curve with an accuracy of ± 3 °C. Additionally ΔT (T$_x$-T$_g$) was calculated, indicating an increased resistance of the glass against crystallization when adding Al$_2$O$_3$ or TiO$_2$. From the thermal properties of the glasses, the addition of Al$_2$O$_3$ and TiO$_2$ is expected to strengthen the phosphate network [30,31]. It should be noted that the Zn glasses have ΔT values below 90 °C, suggesting the poor resistance of

Table 1
Composition and code of the investigated glasses as well as their density and, thermal properties.

x (mol-%) [Code]		ρ (g/cm^3)$\pm$ 0.02 g/cm^3	T_g (°C) ± 3 °C	T_x (°C) ± 3 °C	T_p (°C) ± 3 °C	$\Delta T = T_x - T_g$ (°C)± 6 °C
0.0 [x = 0]		2.63	299	389	417	90
Al$_2$O$_3$	0.75 [0.75Al]	2.63	313	407	446	94
	1.5 [1.5Al]	2.66	324	419	450	95
	3.0 [3Al]	2.66	341	449	474	108
TiO$_2$	0.75 [0.75Ti]	2.63	303	394	421	91
	1.5 [1.5Ti]	2.62	311	429	463	118
	3.0 [3Ti]	2.63	316	448	481	132
ZnO	0.75 [0.75Zn]	2.62	301	384	422	83
	1.5 [1.5Zn]	2.64	300	378	410	78
	3.0 [3Zn]	2.65	303	384	412	81

the Zn glasses to crystallization. DTA curves are shown in Supplementary Fig. 1.

The IR spectra of the glasses are depicted in Fig. 1. The spectra are normalized to the band at 880 cm^{-1}. The spectra are similar to those reported in [18,32].

The structure of glasses can be described using Q^n-units, where n describes the number of bridging oxygens per glass former, e.g. a Q^2 unit would be a phosphorus atom linked to two other phosphorus atoms via connecting oxygen atoms. These glasses are expected to be metaphosphate glasses, as no band is visible at or above 1300 cm^{-1} which would correspond to a (P = O)-bond vibration in a Q^3 unit [33]. A full assignment of the IR bands is presented in [32]. The 600–700 cm^{-1} bands are due to various stretching P-O-(Al/Ti) bands [34, 35] when the Al or Ti ions have placed themselves in the network. The band located at 700–770 cm^{-1} corresponds to the symmetric stretch of P-O-P bridges. The IR bands seen at 1240, ~1090, 880 and 700 cm^{-1} are associated to the ν_{as}(OPO), ν_{ss}(POP), ν_{as}(POP) and ν_{ss}(POP) fundamental vibrations of Q^2 units, respectively [25,36]. The shoulders at 950 cm^{-1} and at 1030 cm^{-1} have been credited to symmetric and antisymmetric (P-O-P) fundamental vibration of Q^2 units in small and large rings [37], and the shoulder at ~1010 cm^{-1} and the band at 1140 cm^{-1} to symmetric and asymmetric stretching vibrations of the PO$_3^{2-}$ in Q^1 units [26].

Compared to the main band, the intensity of the bands at 700–770 cm^{-1} and 1240 cm^{-1} decreases while the bands located at 1010 cm^{-1} and 1140 cm^{-1} increase in intensity with increasing x in the Al and Zn glasses suggesting a progressive increase in the number of Q^1 units at the cost of Q^2 units with the progressive introduction of Al$_2$O$_3$ and ZnO. Similar changes in the phosphate network were reported with the introduction of Al$_2$O$_3$ and ZnO in [16].

In the IR spectra of the Al glasses, the band at 1140 cm^{-1} becomes larger with increasing x. This band may also be related to the creation of P-O-Al bonds at the expense of P-O-P bonds according to [38]. The P-O-Al bonds themselves are seen around 650 cm^{-1} and show the progressive inclusion of Al$_2$O$_3$ to the phosphate network, which contributes to the modification of P = O bond non-bridging oxygens into bridging oxygens. The network connectivity is thus expected to be increased, in agreement with the increase in T_g discussed in the previous section [39]. A shift of the main band at 880 cm^{-1} to longer wavenumbers with increasing Al$_2$O$_3$ is a result of the strengthening of the network by Al ions acting as a network intermediate [39]. Compared to Al, Zn is likely acting as a modifier in our glasses, causing the depolymerization of the
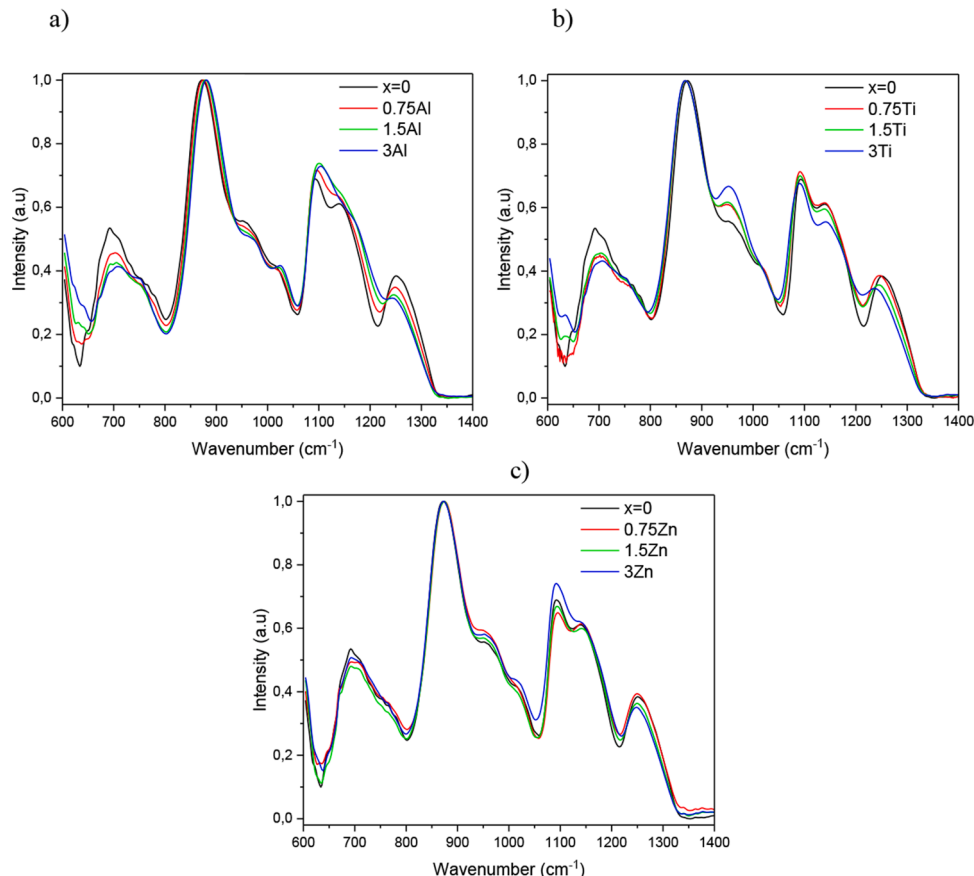
a)

b)

c)

Fig. 1. Normalized IR absorption spectra of Al (a), Ti (b) and Zn(c) glasses.

phosphate network and the reduction in network cross-linking, i.e. less connections between linear phosphate chains, as x increases, which is consistent with the thermal properties of the Zn glasses being similar to those of Zn free one ($x = 0$). Thus, no main band shift is observed.

A reduced IR band at 1090 cm^{-1} and an increased shoulder at 1010 cm^{-1} compared to the main band can be observed with the progressive addition of TiO$_2$ indicating a decrease in the P-O-P bonds because of the formation of P-O-Ti bonds, as explained in [40]. The P-O-Ti bond exhibits a band at around 650 cm^{-1} [38]. Due to its large charge and small ionic radius, Ti ion is expected to place itself between the phosphate rings and chains resulting in Ti–O–P cross-linking between the phosphate tetrahedra and Ti^{4+} ions, reducing the size of the rings as suggested by Navarro et al. [40]. The slight shift observed in the main band position with increasing Ti concentration is likely attributable to P-O-P bond angle changes, as explained in [41]. The increase in T_g confirms the development of 3D network structures by P-O-Ti linkages, as observed in [42].

Fig. 2 presents the absorption spectra of some of the Al, Ti and Zn glasses.

Whereas the Al and Zn glasses exhibit similar optical band gap than the glass with $x = 0$ (Fig. 2a), a shift of the band gap towards longer wavelengths is seen with the introduction of TiO$_2$ (Fig. 2b). This shift is due to the presence of Ti^{4+} ions, which absorb strongly in the UV range [43]. A separate absorption band is visible in the other glasses from 250 to 300 nm when the measurements are obtained from thin samples with a thickness of 0.5 mm. This is caused by various levels of Pt^{4+} contamination from the crucible that occurs during melting [44]. The shape and intensity of the Yb^{3+} absorption band at 980 nm does not appear to be impacted by the addition of Al, Ti, or Zn indicating that the sites of the Yb^{3+} ions are similar in all glasses (Fig. 2c). Table 2 lists the absorption coefficient and cross-section of the glasses.

The absorption spectra were used to calculate the absorption cross-sections at 975 nm using Eq. (1) and were found to be similar to those reported in [18] (Table 2). One should mention that the investigated glasses, independently of their glass composition and doping concentration, exhibit similar absorption and emission cross-sections at 975 nm, within the measurement accuracy confirming that the local Yb^{3+} ions environment in the Al/Ti/Zn glasses are close to that of the parent glass ($x = 0$) and only weak changes in the Yb^{3+} coordination sites are expected when changing the glass composition.

As in [18], the glasses were thermally treated individually for 17 h at (T_g+20 °C), followed by 2 h at T_p. After the thermal treatment, all the glasses were opaque due to surface crystallization that occurred during

Table 2
Optical properties of the investigated glasses.

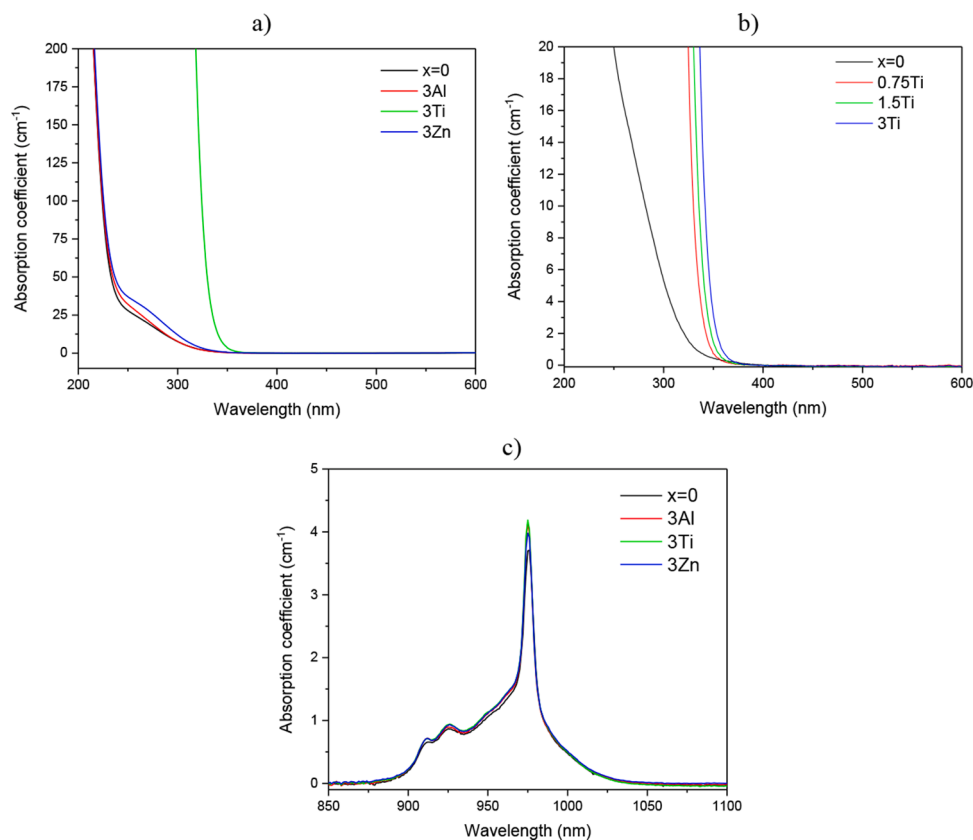| x (mol-%)[Code]		Yb^{3+}(ions/ cm^3)(10^{20}) $\pm$ 5%	α_{abs} at 975 nm (cm^{-1})	σ_{abs} at 975 nm(10^{-21} cm^2)$\pm$ 10%	σ_{emi} at 975 nm(10^{-21} cm^2)$\pm$ 20%
0.0 [$x = 0$]		3.89	3.91	9.87	3.72
Al$_2$O$_3$	0.75 [0.75Al]	3.92	3.91	9.97	4.88
	1.5 [1.5Al]	3.98	4.11	10.33	5.28
	3.0 [3Al]	3.97	4.17	10.51	5.33
TiO$_2$	0.75 [0.75Ti]	3.94	3.95	10.02	4.92
	1.5 [1.5Ti]	3.92	3.93	10.03	5.05
	3.0 [3Ti]	3.94	4.22	10.70	4.98
ZnO	0.75 [0.75 Zn]	3.93	3.86	9.83	4.28
	1.5 [1.5 Zn]	3.94	3.66	9.29	4.13
	3.0 [3 Zn]	3.96	3.98	10.04	4.56

Fig. 2. Absorption spectrum of the glasses prepared with 3-mol% of Al$_2$O$_3$, TiO$_2$ and ZnO (thickness: 0.5 mm) (a), absorption spectrum of the Ti glasses (b) and absorption band centered at 980 nm of the glasses prepared with 3-mol% of Al$_2$O$_3$, TiO$_2$ and ZnO (thickness: 1.7 mm) (c).

the thermal treatment as confirmed using XRD (Fig. 3).

The XRD patterns show peaks which can be assigned to $NaPO_3$ [ICDD 00–011–0648], $NaYb(P_2O_7)$ [ICDD 04–014–6349], $Na_5P_3O_{10}$ [ICDD 00–010–0179] and $Na_2H_2(PO_3)_4$ [ICDD 00–009–0100] as reported in [18]. No noticeable changes in the XRD pattern occur when adding Zn in the glass. However, a reduction in intensity of the peaks associated to $NaYb(P_2O_7)$ phase (especially peaks at 16.5° and 24.9°, □) and to $NaPO_3$ phase (especially peaks at 20°, 26.8° and 30.5°, ■) relative to the peaks associated with $Na_5P_3O_{10}$ is visible with increasing in x in the Al and Ti glasses, with the change being smaller in the XRD pattern of the Ti glasses. The delay in the precipitation and growth of $NaYb(P_2O_7)$ and $NaPO_3$ nuclei due to the introduction of Al_2O_3, and to a much lesser degree TiO_2, is coherent with a higher mobility of the cationic species due to a lower reticulation of the phosphate network in agreement with shortened P-O-P chains. It is the P-O-Al/Ti bond formation which is thought to promote the precipitation of the $Na_5P_3O_{10}$ crystals while inhibiting the migration of Yb^{3+} ions and thus the precipitation of $NaYb(P_2O_7)$ and $NaPO_3$ phases. As explained in the previous section, Zn is suspected to act as a modifier in the glass network and so has no impact on the nucleation and growth mechanism.

The presence of $Na_2H_2(PO_3)_4$ phase might be correlated with the glasses' resistance to water absorption as this (hydrated) crystal phase is the most visible in the XRD pattern of the $x = 0$ glass (peak at around 18°, +) and much less in the XRD pattern of the other glasses. XRD patterns of the as-prepared glasses (Supplementary Fig. 2) were found to show completely amorphous glasses with no traces of unmelted precursors.

Figs. 4a, c and e show the Yb^{3+} emission spectra of the as-prepared

Al, Ti and Zn glasses, respectively. They are normalized at the maximum of the zero-line transition at around 975 nm. The as-prepared glasses exhibit similar emission band which exhibits a prominent main band at 975 nm with a broad shoulder around 1 μm resulting from the radiative de-excitation down to the different Stark component of the ground state manifold. The emission band has a shape which is typical of Yb^{3+} ions located in a glassy, amorphous matrix meaning that the contribution of the different radiative contribution is smoothed into a wide envelop ranging from 980 nm to 1075 nm [45]. The glasses exhibit similar emission band and similar integrated emission area of the Yb^{3+} emission band. The global emission as well as the Yb^{3+} environment seems not be affected by the addition of Al, Ti or Zn in a good agreement with the calculated absorption and emission cross-sections listed in Table 2.

The emission spectra of the thermally treated glasses are shown in Fig. 4b, d, f for Al, Ti and Zn glasses, respectively. The shape of the emission changes after thermal treatment as the shoulder at ~1 μm is more pronounced relative to the band located at 975 nm. This experimental distortion of the spectral distribution is the consequence of the zero-line reabsorption by the lower energy components. A relative decrease in intensity of the ~1 μm line reflects a lower interaction between Yb^{3+} ions in agreement with a lower concentration of $NaYb(P_2O_7)$ or smaller $NaYb(P_2O_7)$ grains into the Al doped glasses in agreement with the XRD patterns. This is also associated to an increase of the Yb^{3+} intensity within the heat-treated glasses with increasing Al_2O_3 content. The thermal treatment results in reduced total Yb^{3+} emission intensity area, as seen in Fig. 4g where the values for heat treated samples (points) are significantly lower than those of the as-prepared, untreated glass
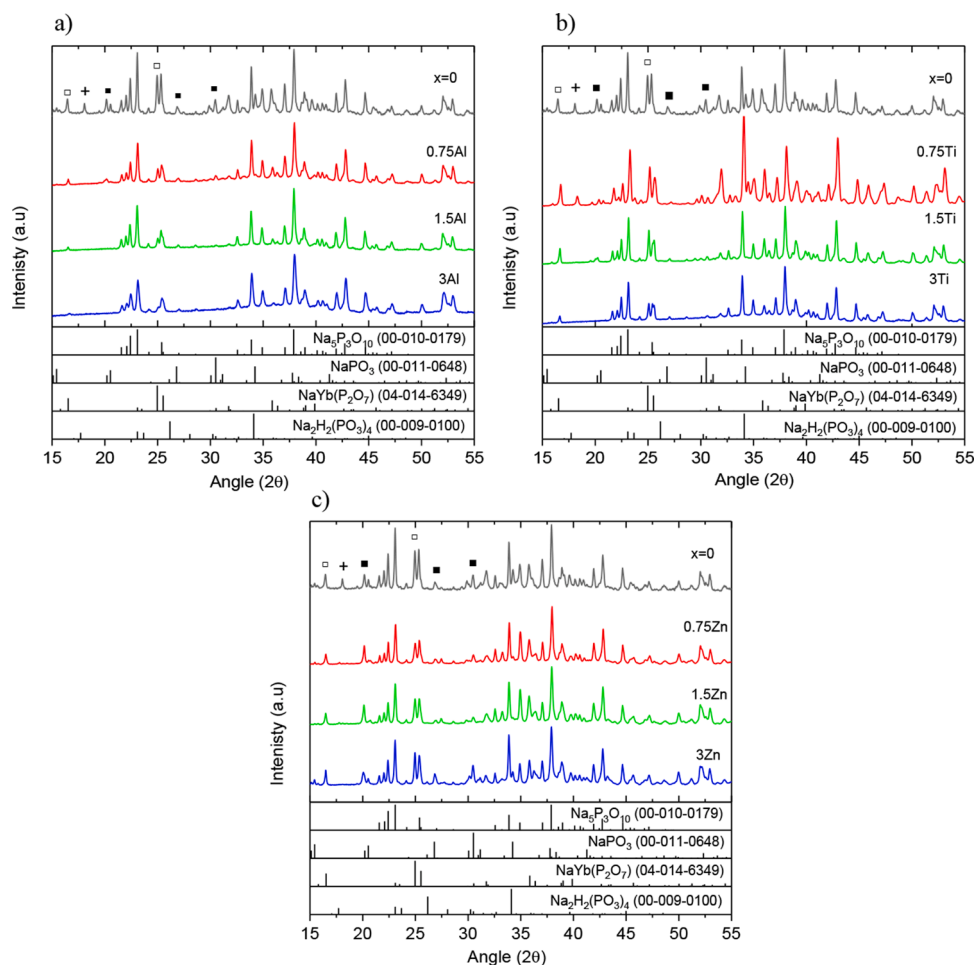

Fig. 3. XRD patterns of Al_2O_3 (a), TiO_2 (b), and ZnO (c) glasses after 17 h at T_g+20 °C and 2 h at T_p and reference patterns for $Na_5P_3O_{10}$, $NaPO_3$, $NaYb(P_2O_7)$.
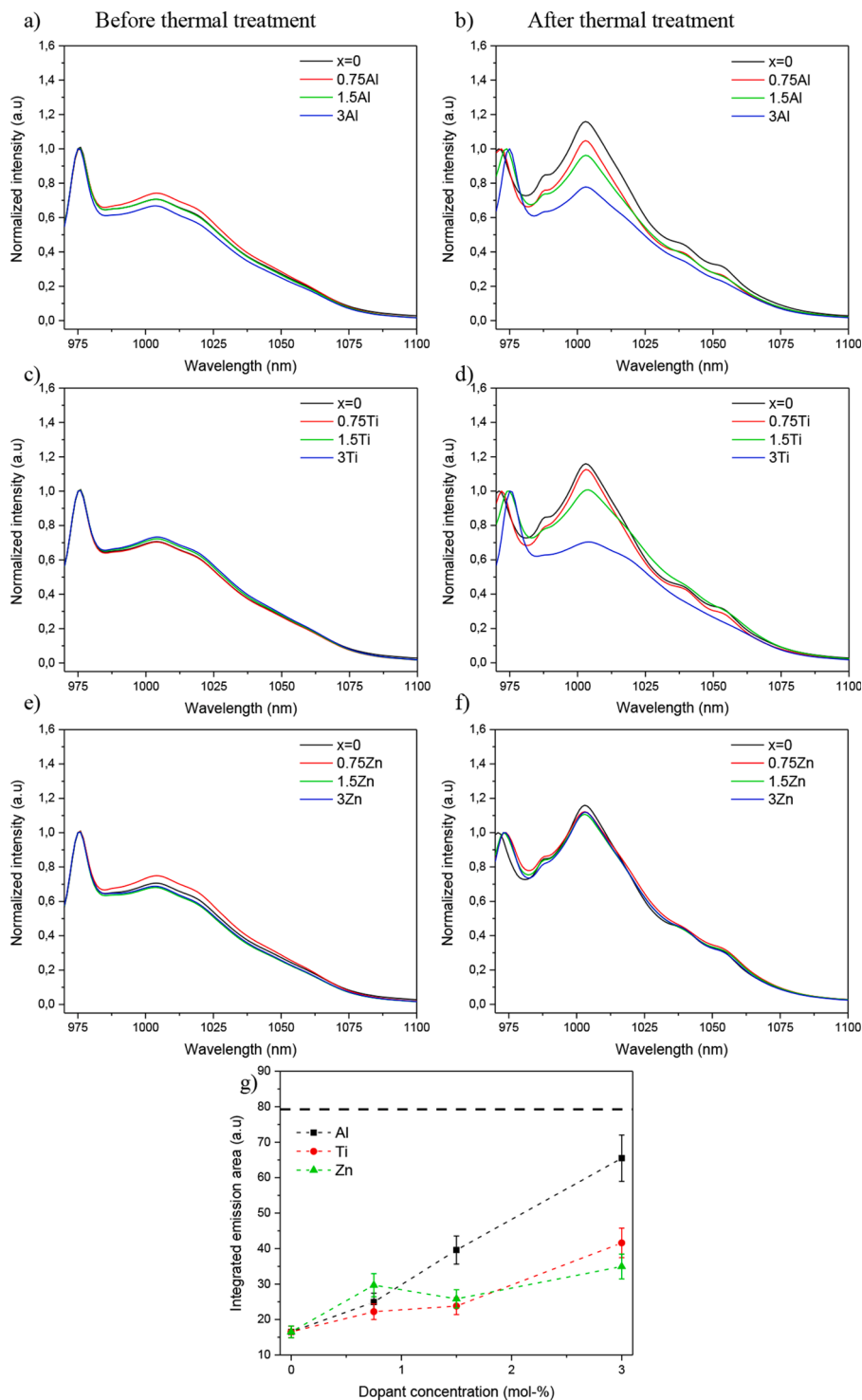
Fig. 4. Normalized emission band of the Al (a, b), Ti (c, d), and Zn (e, f) glasses before and after thermal treatment at (T_g+20 °C) for 17 h and at T_p for 2 h, respectively. Subplot 4 g shows integrated emission area of the glasses' Yb^{3+} emission band after a thermal treatment at (T_g+20 °C) for 17 h and at T_p for 2 h. The dashed horizontal line shows the integrated emission area of the as-prepared, untreated glass. (λ_{exc}= 965 nm).

(dashed line). Comparable changes in the Yb^{3+} spectroscopic properties due to similar thermal treatment were reported in [18] and were associated to the crystallization of the $NaYb(P_2O_7)$ crystals. The relative increase in the intensity of the shoulder and the simultaneous the reduction in the Yb^{3+} emission area is associated with the higher NaYb (P_2O_7) content. The Ti glasses show the same spectral evolution as the Al glasses, as opposed to the Zn glasses, for which the shape of the emission remains constant. This confirms the different role of Al/Ti and Zn onto

the structure of the glass matrix and on the change in the $NaYb(P_2O_7)$ concentration and/or grain size.

Considering the whole series of glasses, these changes in the Yb^{3+} spectroscopic properties are related to the $Na_5P_3O_{10}$ phase precipitating at the expense of $NaYb(P_2O_7)$ when changing the glass composition. The addition of Zn results in a higher cation migration that allows the precipitation of fewer $NaYb(P_2O_7)$ crystalline grains and thus the shape of the emission is similar to that of thermally treated $x = 0$ glass. On the

contrary, when adding Al and Ti, the glass network remains quite rigid limiting the migration of Yb and thus favors the growth of bigger particles of NaYb(P$_2$O$_7$) for the lowest x. However, the evolution in the emission intensity after heat treatment seems to indicate that the concentration the NaYb(P$_2$O$_7$) grains must be different within these glasses.

It is commonly known that the hydroxyl groups can act as a luminescent quencher of Yb^{3+} ions [46], the IR spectra of the glasses were measured after the quenching and after 5 months. Fig. 5 exhibits similar broad band than the one reported in [18]. This band is associated to free, weakly associated hydroxyl groups at around 3500 cm^{-1} and to strongly associated hydroxyl groups at 2800 cm^{-1} [18]. One should point out that the absorption coefficient at 2790 cm^{-1} of the $x = 0$ glass was found to be within 10% of the one reported in [18], confirming that this glass can be prepared repeatedly with the same amount of OH. The addition of Al$_2$O$_3$, TiO$_2$ or ZnO decreases the intensity of the OH band indicating a reduction in the OH content independent of the doping rate. This effect might be more pronounced for the Zn glasses as Zn acts as a modifier, the linear phosphate chain length in the Zn glasses is expected to be longer than in the $x = 0$ glass which reduces the OH content as suggested in [47]. The Fig. 5 also depicts the IR spectra of the glasses measured 5 months after synthesis (dashed thick line). One should mention that the glasses were kept in dried atmosphere during this time. Whereas no noticeable changes in the intensity of the OH band was observed in the Al, Ti and Zn glasses, the intensity of the OH band in the spectrum of the $x = 0$ glass increases slightly, indicative of an absorption of water over time. Thus, these newly developed glasses appear to be also more stable against water absorption over time than the $x = 0$ glass probably due to their strengthened network (Al and Ti glasses) or to their long phosphate chains (Zn glass) as discussed previously.

The investigated glasses were thermally treated at (T$_g$+20 °C) for 17 h, followed by a treatment at (T$_p$ - 40 °C) for 30 min in order to verify if their crystallization also occurs in bulk and from surface. After the thermal treatment, all glasses showed surface crystallization as depicted in Fig. 6a, the thickness of which was composition dependent (Fig. 6b).

The crystals have the similar needle-like shape than the crystals precipitating in the $x = 0$ glass and consist mainly of Na$_5$P$_3$O$_{10}$ [18], shown in Fig. 6. Additionally, the addition of Al$_2$O$_3$, TiO$_2$ and ZnO in the phosphate network changed the crystallization process as no bulk crystallization was found in the newly developed glasses except for the 0.75Al glass, in which few crystals could been seen in the volume of the glass with an optical microscope.

The addition of Al$_2$O$_3$, TiO$_2$ and ZnO in the phosphate network increases the thickness of the crystallized surface layer, clearly showing that the newly developed glasses are more prone to crystallization than the glass with $x = 0$. One should point out that the thickness of the crystallized layer is thinner in the Zn glasses than in the other glasses indicating a difference in the growth of the crystalline particles; increased number of crystalline nuclei and/or their higher distribution in the crystallized layer, favored by a lower P-O-P connectivity. It is the increased connectivity by the P-O-Al/Ti bond formation at the cost of the P-O-P bonds which is thought to promote the surface crystallization.

4. Conclusions

New Yb^{3+} doped phosphate glasses were developed to understand the impact of Al$_2$O$_3$, TiO$_2$ and ZnO addition on the formation of transparent Yb^{3+} doped phosphate glass-ceramic. While Al$_2$O$_3$, TiO$_2$ and ZnO do not directly impact the Yb^{3+} site significantly, their addition in the phosphate network results in the breakage of P-O-P bonds, with the replacement of P-O-P bonds by P-O-Al/Ti bonds when adding Al$_2$O$_3$ or TiO$_2$ or in the formation of longer, more linear phosphate chains when adding ZnO. Al, Ti and Zn contribute to the reduction in the number of hydroxyl groups present in the glass but also improve the glasses' resistance against water absorption over time. While the addition of Al and Ti increases the hot working range of the glass as demonstrated by the increased ΔT, they also increase the crystallization kinetics as seen by the increased surface layer thickness in Al$_2$O$_3$ and TiO$_2$ glasses after the thermal treatment. The addition of Al$_2$O$_3$, TiO$_2$ and ZnO was found
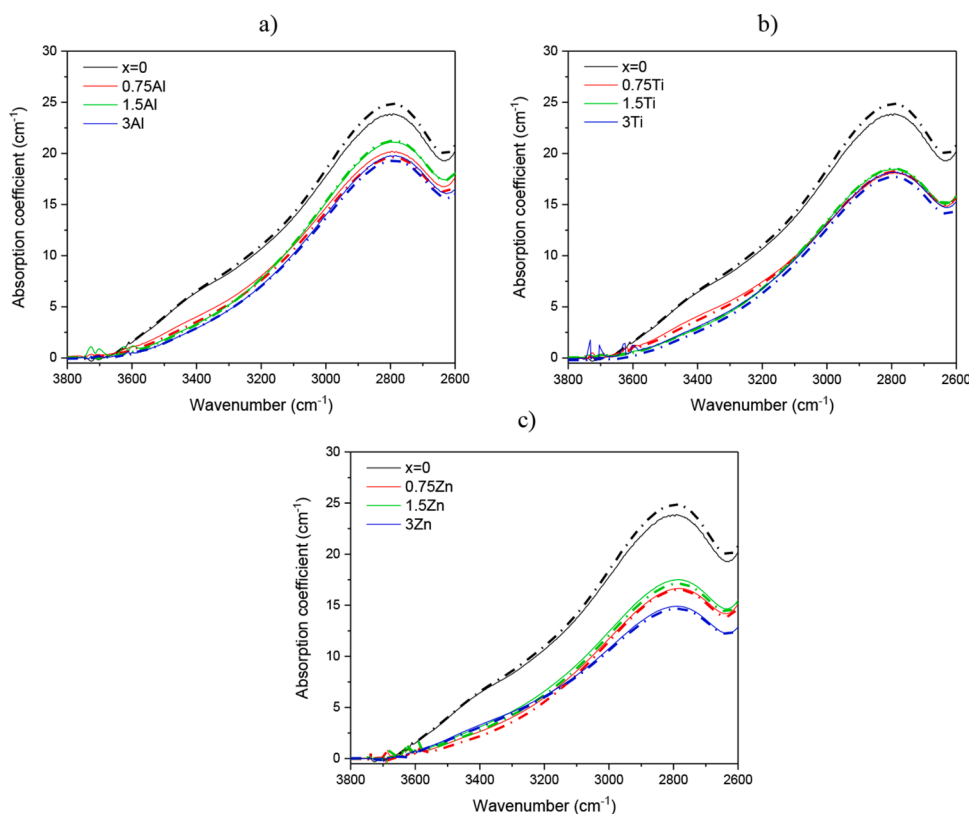

Fig. 5. IR absorption spectra of the Al (a), Ti(b), and Zn(c) glasses measured after melting (solid line) and after 5 months (dashed thick line).

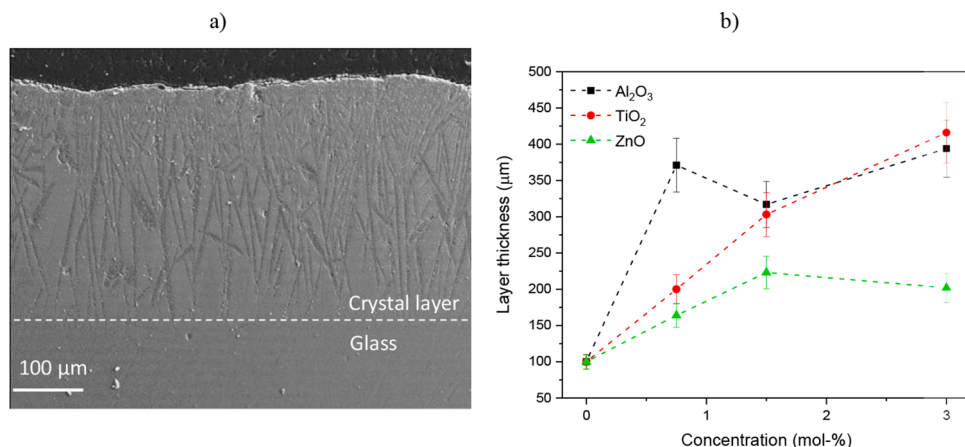a)   b)

Fig. 6. SEM image of surface crystal layer in Ti 1.5% glass after thermal treatment (a), taken as an example, and the crystalline layer thickness as a function of x (b).

to have an impact on the nucleation and growth process as it promotes not only the precipitation of $Na_5P_3O_{10}$ phase at the expense of the $NaYb(P_2O_7)$ and $NaPO_3$ phases but also the surface crystallization at the expense of the bulk crystallization.

CRediT authorship contribution statement

Mikko Hongisto: Conceptualization, Investigation, Formal analysis, Resources, Data curation, Writing – original draft, Writing – review & editing, Visualization. **Otto Linros:** Investigation, Resources, Visualization. **Sylvain Danto:** Writing – review & editing. **Veronique Jubera:** Writing – review & editing. **Laeticia Petit:** Writing – review & editing, Supervision.

Declaration of Competing Interest

The authors declare that they have no known competing financial interests or personal relationships that could have appeared to influence the work reported in this paper.

Data Availability

Data will be made available on request.

Supplementary materials

Supplementary material associated with this article can be found, in the online version, at doi:10.1016/j.materresbull.2022.112032.

References

[1] J. Limpert, T. Schreiber, T. Clausnitzer, K. Zöllner, H.-.J. Fuchs, E.-.B. Kley, H. Zellmer, A. Tünnermann, High-power femtosecond Yb-doped fiber amplifier, Opt. Express 10 (2002) 628, https://doi.org/10.1364/oe.10.000628.

[2] L.D. DeLoach, S.A. Payne, L.L. Chase, L.K. Smith, W.L. Kway, W.F. Krupke, Evaluation of absorption and emission properties of yb^{3+} doped crystals for laser applications, IEEE J. Quantum Electron. 29 (1993) 1179–1191, https://doi.org/10.1109/3.214504.

[3] Xu, S.; Yang, Z.; Zhang, W.; Wei, X.; Qian, Q.; Chen, D.; Zhang, Q.; Shen, S.; Peng, M.; Qiu, J. 400 mW ultrashort cavity low-noise single-frequency Yb3+-doped phosphate fiber laser. Opt. Lett.2011, 36, 3708, doi:10.1364/ol.36.003708.

[4] W. Santos, A. de Camargo, D. Wu, W. Silva, L. Zhang, C. Jacinto, Cooperative upconversion, radiation trapping, and self-quenching effects in highly yb^{3+} -doped oxyfluoride glasses, Sci. Adv. Mater. 5 (2013) 1948–1953, https://doi.org/10.1166/sam.2013.1661.

[5] C. Yu, B. Chen, Z. Xizhen, X. Li, J. Zhang, S. Xu, H. Yu, J.-.S. Sun, Y. Cao, H. Xia, Influence of Er^{3+} concentration and Ln^{3+} on the Judd-Ofelt parameters in LnOCl (Ln = Y, La, Gd) phosphors, Phy. Chem. Chem. Phys. (2020) 22, https://doi.org/10.1039/C9CP06755H.

[6] J. Sablayrolles, V. Jubera, F. Guillen, R. Decourt, M. Couzi, J.P. Chaminade, A. Garcia, Infrared and visible spectroscopic studies of the ytterbium doped borate Li$_6$Y(BO$_3$)$_3$, Opt. Commun. 280 (2007) 103–109, https://doi.org/10.1016/J.OPTCOM.2007.07.034.

[7] V. Jubera, J. Sablayrolles, F. Guillen, R. Decourt, M. Couzi, A. Garcia, From the infrared to the visible range: spectroscopic studies of ytterbium doped oxyborates, Opt. Commun. 282 (2009) 53–59, https://doi.org/10.1016/j.optcom.2008.09.075.

[8] V. Venkatramu, R. Vijaya, S.F. León-Luis, P. Babu, C.K. Jayasankar, V. Lavín, L.J. Dhareshwar, Optical properties of Yb^{3+}-doped phosphate laser glasses, J. Alloys Compd. 509 (2011) 5084–5089, https://doi.org/10.1016/j.jallcom.2011.01.148.

[9] B. Schaudel, P. Goldner, M. Prassas, F. Auzel, Cooperative luminescence as a probe of clustering in Yb^{3+} doped glasses, J. Alloys Compd. 300 (2000) 443–449, https://doi.org/10.1016/S0925-8388(99)00760-4.

[10] P. Goldner, B. Schaudel, M. Prassas, Dependence of cooperative luminescence intensity on Yb^{3+} spatial distribution in crystals and glasses, Phys. Rev. B 65 (2002) 1–10, https://doi.org/10.1103/PhysRevB.65.054103.

[11] S. Xu, Z. Yang, W. Zhang, X. Wei, Q. Qian, D. Chen, Q. Zhang, S. Shen, M. Peng, J. Qiu, 400 mW ultrashort cavity low-noise single-frequency Yb^{3+}-doped phosphate fiber laser, Opt. Lett. 36 (2011) 3708, https://doi.org/10.1364/ol.36.003708.

[12] R. Sen, N.N.G. Boetti, M. Hokka, L. Petit, Optical, structural and luminescence properties of oxyfluoride phosphate glasses and glass-ceramics doped with Yb^{3+}, J. Non-Crystalline Solids X (2019) 1, https://doi.org/10.1016/j.nocx.2018.100003.

[13] N.G.Boetti Nommeots-Nomm, T. Salminen, J. Massera, M. Hokka, L. Petit, Luminescence of Er^{3+} doped oxyfluoride phosphate glasses and glass-ceramics, J. Alloys Compd. 751 (2018) 224–230, https://doi.org/10.1016/j.jallcom.2018.04.101.

[14] Setsuhisa Tanabe, Hideaki Hayashi, Teiichi Hanada, Noriaki Onodera, Fluorescence properties of Er^{3+} ions in glass ceramics containing LaF$_3$ nanocrystals, Opt Mater (Amst) 19 (2002) 343–349, https://doi.org/10.1016/S0925-3467(01)00236-1.

[15] Xvsheng Qiao, Xianping Fan, Jin Wang, Minquan Wang, Luminescence behavior of Er^{3+} ions in glass–ceramics containing CaF$_2$ nanocrystals, J. Non. Cryst. Solids 351 (2005) 357–363, https://doi.org/10.1016/j.jnoncrysol.2004.11.021.

[16] P. Lopez-Iscoa, L. Petit, J. Massera, D. Janner, N.G. Boetti, D. Pugliese, S. Fiorilli, C. Novara, F. Giorgis, D. Milanese, Effect of the addition of Al$_2$O$_3$, TiO$_2$ and ZnO on the thermal, structural and luminescence properties of Er^{3+}-doped phosphate glasses, J. Non. Cryst. Solids 460 (2017) 161–168, https://doi.org/10.1016/j.jnoncrysol.2017.01.030.

[17] X. Qiao, X. Fan, Y. Pan, A. Lotnyk, L. Kienle, Microstructure and luminescence of Yb^{3+}-doped fluorosilicate glass ceramics, Mater. Res. Bull. 47 (2012) 29–34, https://doi.org/10.1016/j.materresbull.2011.10.014.

[18] M. Hongisto, A. Veber, N.G. Boetti, S. Danto, V. Jubera, L. Petit, Transparent Yb^{3+} doped phosphate glass-ceramics, Ceram. Int. 46 (2020) 26317–26325, https://doi.org/10.1016/j.ceramint.2020.01.121.

[19] E.S. Filho, K.V. Krishnaiah, Y. Ledemi, Y. Yu, Y. Messaddeq, G. Nemova, R. Kashyap, Ytterbium-doped glass-ceramics for optical refrigeration, *Opt. Express* 23 (2015) 4630–4640, https://doi.org/10.1364/OE.23.004630.

[20] T. Meyneng, J. Thomas, Y. Ledemi, M. Allix, E. Veron, C. Genevois, R. Kashyap, Y. Messaddeq, The role of fluorine in high quantum yield oxyfluoride glasses and glass-ceramics, J. Alloys Compd. 900 (2022), 163512, https://doi.org/10.1016/j.jallcom.2021.163512.

[21] Q. Luo, X. Qiao, X. Fan, Zhang, X, Near-infrared emission of Yb^{3+} through energy transfer from ZnO to Yb^{3+} in glass ceramic containing ZnO nanocrystals, Opt. Lett. 36 (2011) 2767–2769, https://doi.org/10.1364/OL.36.002767.

[22] A. Abdelouas, J. Neeway, B. Grambow, Chemical Durability of Glasses. Springer Handbooks, Springer, 2019, pp. 407–438, https://doi.org/10.1007/978-3-319-93728-1_12.

[23] S. Krimi, A. El Jazouli, L. Rabardel, M. Couzi, I. Mansouri, G. Le Flem, Glass formation in the $Na_2O\text{-}TiO_2\text{-}P_2O_5$ system, J. Solid State Chem. 102 (1993) 400–407, https://doi.org/10.1006/jssc.1993.1051.

[24] R.K. Brow, Review: the structure of simple phosphate glasses, J. Non. Cryst. Solids 263 (2000) 1–28, https://doi.org/10.1016/S0022-3093(99)00620-1.

[25] R.K. Brow, Nature of alumina in phosphate glass: i, properties of sodium aluminophosphate glass, J. Am. Ceram. Soc. 76 (1993) 913–918, https://doi.org/10.1111/j.1151-2916.1993.tb05315.x.

[26] R.K. Brow, D.R. Tallant, S.T. Myers, C.C. Phifer, The short-range structure of zinc polyphosphate glass, J. Non. Cryst. Solids 191 (1995) 45–55, https://doi.org/10.1016/0022-3093(95)00289-8.

[27] R. Brow, D. Tallant, W. Warren, A. McIntyre, D. Day, Spectroscopic Studies of the Structure of Titanophosphate and Calcium Titanophosphate Glasses, Phys. Chem. Glas. (1997).

[28] W.F. Krupke, Induced-Emission Cross Sections in Neodymium Laser Glasses, IEEE J. Quantum Electron. 10 (1974) 450–457, https://doi.org/10.1109/JQE.1974.1068162.

[29] M.J. Weber, Probabilities for radiative and nonradiative decay of Er^{3+} in LaF_3, Phys. Rev. 157 (1967) 262–272, https://doi.org/10.1103/PhysRev.157.262.

[30] S. Sandhu, D. Singh, S. Kumar, R. Thangaraj, Estimation of glass transition temperature of $Al_x(Ge_2Sb_2Te_5)_{1-x}$ glassy system, J. Ovonic Res. 9 (2013) 143–146.

[31] E.A. Abou Neel, W. Chrzanowski, S.P. Valappil, L.A. O'Dell, D.M. Pickup, M. E. Smith, R.J. Newport, J.C Knowles, Doping of a high calcium oxide metaphosphate glass with titanium dioxide, J. Non. Cryst. Solids 355 (2009) 991–1000, https://doi.org/10.1016/j.jnoncrysol.2009.04.016.

[32] N. Ojha, M. Tuomisto, M. Lastusaari, L. Petit, Upconversion from fluorophosphate glasses prepared with $NaYF_4$:er^{3+},Yb^{3+} nanocrystals, RSC Adv 8 (2018) 19226–19236, https://doi.org/10.1039/c8ra03298j.

[33] K. Meyer, Characterization of the structure of binary zinc ultraphosphate glasses by infrared and Raman spectroscopy, J. Non. Cryst. Solids 209 (1997) 227–239, https://doi.org/10.1016/S0022-3093(96)00563-7.

[34] S.V. Stefanovsky, O.I. Stefanovsky, M.I. Kadyko, I.A. Presniakov, B.F. Myasoedov, The effect of Fe_2O_3 substitution for Al_2O_3 on the phase composition and structure of sodium–aluminum–iron phosphate glasses, J. Non. Cryst. Solids 425 (2015) 138–145, https://doi.org/10.1016/j.jnoncrysol.2015.05.039.

[35] Mingwei Lu, Fu Wang, Qilong Liao, Kuiru Chen, Jianfa Qin, Sheqi Pan, FTIR spectra and thermal properties of TiO_2-doped iron phosphate glasses, J. Mol. Struct. 1081 (2015) 187–192, https://doi.org/10.1016/j.molstruc.2014.10.029.

[36] E. Metwalli, R.K. Brow, Modifier effects on the properties and structures of aluminophosphate glasses, J. Non. Cryst. Solids 289 (2001) 113–122, https://doi.org/10.1016/S0022-3093(01)00704-9.

[37] J.A. Wilder, J.E. Shelby, Property variation in alkali alkaline-earth metaphosphate glasses, J. Am. Ceram. Soc. 67 (1984) 438–444, https://doi.org/10.1111/j.1151-2916.1984.tb19732.x.

[38] J.Y. Ding, P.Y. Shih, S.W. Yung, K.L. Hsu, T.S. Chin, The properties and structure of Sn-Ca-P-O-F glasses, Mater. Chem. Phys. 82 (2003) 61–67, https://doi.org/10.1016/S0254-0584(03)00161-5.

[39] Y.B. Saddeek, M.A. Kaid, M.R. Ebeid, FTIR and physical features of Al_2O_3-La_2O_3-P_2O_5-PbO glasses, J. Non. Cryst. Solids 387 (2014) 30–35, https://doi.org/10.1016/j.jnoncrysol.2013.12.029.

[40] M. Navarro, M.-.P. Ginebra, J. Clément, M. Salvador, A. Gloria, J.A. Planell, Physicochemical degradation of titania-stabilized soluble phosphate glasses for medical applications, J. Am. Ceram. Soc. 86 (2003) 1345–1352, https://doi.org/10.1111/j.1151-2916.2003.tb03474.x.

[41] Mingwei Lu, Fu Wang, Qilong Liao, Kuiru Chen, Jianfa Qin, Sheqi Pan, FTIR spectra and thermal properties of TiO_2-doped iron phosphate glasses, J. Mol. Struct. 1081 (2015) 187–192, https://doi.org/10.1016/j.molstruc.2014.10.029.

[42] H. Segawa, N. Akagi, T. Yano, S. Shibata, Properties and structures of TiO_2–ZnO–P_2O_5 glasses, J. Ceram. Soc. Japan 118 (2010) 278–282, https://doi.org/10.2109/jcersj2.118.278.

[43] L.H.C. Andrade, S.M. Lima, A. Novatski, A.M. Neto, A.C. Bento, M.L. Baesso, F.C. G. Gandra, Y. Guyot, G. Boulon, Spectroscopic assignments of Ti^{3+} and Ti^{4+} in titanium-doped OH- free low-silica calcium aluminosilicate glass and role of structural defects on the observed long lifetime and high fluorescence of Ti3+ ions, Phys. Rev. B - Condens. Matter Mater. Phys. (2008) 78, https://doi.org/10.1103/PHYSREVB.78.224202/.

[44] C.A. Click, R.K. Brow, P.R. Ehrmann, J.H. Campbell, Characterization of Pt4+ in alumino-metaphosphate laser glasses, J. Non. Cryst. Solids 319 (2003) 95–108, https://doi.org/10.1016/S0022-3093(02)01962-2.

[45] L. Zhang, Y. Xia, X. Shen, R. Yang, W. Wei, Investigations on the effects of the Stark splitting on the fluorescence behaviors in Yb^{3+}-doped silicate, tellurite, germanate, and phosphate glasses, Opt. Mater. (Amst) 75 (2018) 1–6, https://doi.org/10.1016/j.optmat.2017.10.008.

[46] H. Ohkawa, H. Hayashi, Y. Kondo, Influence of water on non-radiative decay of Yb^{3+} $^2F_{5/2}$ level in phosphate glass, Opt. Mater. (Amst) 33 (2010) 128–130, https://doi.org/10.1016/j.optmat.2010.10.027.

[47] C.Z. Weng, J.H. Chen, P.Y. Shih, Effect of dehydroxylation on the structure and properties of $ZnCl_2$-ZnO-P_2O_5 glasses, Mater. Chem. Phys. 115 (2009) 628–631, https://doi.org/10.1016/j.matchemphys.2009.01.022.